

Efficient spatially resolved multimode quantum memory

K. Surmacz, J. Nunn, K. Reim, K. C. Lee, V. O. Lorenz, B. Sussman, I. A. Walmsley, and D. Jaksch
Clarendon Laboratory, University of Oxford, Parks Road, Oxford OX1 3PU, United Kingdom

(Received 30 March 2007; published 8 September 2008)

Light storage in atomic ensembles has been implemented successfully, but the retrieval efficiency can be low. We propose to improve this efficiency with appropriately phase-matched backward propagating retrieval. This method allows for easy spatial filtering of the retrieved light; in addition, multiple optical modes can be stored in the transverse momentum of the ensemble. We model walk-off effects with a full numerical simulation, and confirm the applicability of the scheme.

DOI: [10.1103/PhysRevA.78.033806](https://doi.org/10.1103/PhysRevA.78.033806)

PACS number(s): 42.50.Gy, 42.50.Ct, 42.50.Ex

I. INTRODUCTION

Atomic ensembles represent an increasingly useful tool for manipulating the propagation [1] and quantum state [2] of optical fields. In particular, the existence of long-lived coherences affords the ability to temporarily store a light pulse as a stationary excitation within an ensemble. This kind of storage preserves quantum correlations [3–5] and forms a key component in the technology required for the implementation of quantum communication protocols [6,7] and quantum computing architectures [8]. The optimization of the efficiency of storage into, and retrieval from, such a quantum memory is the subject of intense research [9–11], since the utility of the technology ultimately depends on the favorable scaling of losses for memories operated in series.

In this paper, we present a simple scheme to improve the efficiency of retrieval from an ensemble quantum memory; we check our predictions against a full numerical simulation, and we consider a generalization of the procedure to the storage of multiple optical modes. We will show that high efficiency can be achieved provided the optical fields involved are not focused too tightly, and that the use of wide collimated beams, if sufficient intensity is available, allows for efficient multimode storage.

First we introduce the standard storage protocol, and we discuss the factors limiting the efficiency of retrieval from a memory. In the following, we neglect a class of ensemble memories based on photon echoes [9,12], to which our scheme is not directly applicable (although the problems outlined below persist; other techniques are required to address them [13,14]). We also omit any discussion of continuous variable quantum memories [15–18].

II. SYSTEM

A simple system in which light can be stored for extended periods consists of an ensemble of identical three-level atoms with a Λ -type structure [see Fig. 1(a)]. The excited state $|2\rangle$ is coupled strongly to the electromagnetic field, but is therefore noisy and short-lived, with a coherence lifetime characterized by the decay rate γ . The metastable state $|3\rangle$ has no strong couplings to the state $|1\rangle$, and is long-lived. At the start of the memory interaction, all the atoms are in state $|1\rangle$, which we call the *initial* state. Later we will see that certain advantages accrue when $|1\rangle$ lies energetically *above*

$|3\rangle$, although this is somewhat nonstandard. An incident signal pulse is stored as an excitation of the state $|3\rangle$; the interaction is mediated by the state $|2\rangle$, which provides the strong coupling necessary for efficient storage. In general, this is accomplished by the application of an intense auxiliary control field tuned into two-photon resonance with the signal field, as shown in Fig. 1(a). If both signal and control fields are resonant with the excited state, storage is realized via electromagnetically induced transparency (EIT) [19–22], in which adiabatic reduction of the intensity of the control field dynamically slows the signal field to a standstill. If the fields are detuned far from resonance by a common detuning Δ , the signal field is coherently absorbed in a two-photon Raman interaction [11,23–25]. In both cases, the signal field is mapped to a collective excitation known as a *spin wave*, with a wave function whose spatial distribution over the ensemble depends on the transverse profile and temporal shape of the control and signal pulses. Some time later, the stored excitation may be converted back into an optical pulse by a second application of the control field.

For the case in which the signal and control pulses propagate in the same direction, a one-dimensional analysis predicts the control pulse shape that maximizes the storage efficiency [24,25], and this kind of optimization for EIT has recently been successfully demonstrated in the laboratory [26,27]. In general, the shape of the spin wave generated by the optimized storage process is highly asymmetric along the propagation direction [see the inset of Fig. 1(b)], as might be expected from Beer's-law absorption. The spin wave amplitude is large at the input face of the ensemble, but decays away toward the exit face. By contrast, the retrieval process is optimized when the spin wave has the complementary

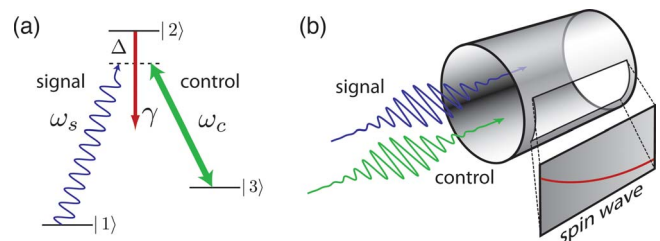


FIG. 1. (Color online) (a) The level structure of the atoms in a typical ensemble memory. (b) A schematic of the storage process, in which an incident signal field is converted to a distributed excitation within the ensemble known as a spin wave.

shape, with a small initial amplitude growing with propagation distance, consistent with a description of the retrieval of the signal field as a straightforward gain process. If retrieval is attempted in the forward direction, the efficiency is limited by poor overlap of the generated spin wave with the optimal one. The above argument suggests that backward retrieval should be preferable, since in this case the input and exit faces of the ensemble are switched, and the generated spin wave is optimal for retrieval. This space-reversal symmetry is a direct consequence of the time-reversal symmetry of the Hamiltonian dynamics that govern the interaction [24,25].

However, a difficulty arises if the energies of the states $|3\rangle$ and $|1\rangle$ are different. In that case, the frequencies ω_s , ω_c of the signal and control fields differ, and the difference in their momenta is taken up by the spin wave, which therefore acquires a spatially varying phase. If this phase is not conjugated before backward retrieval is attempted, the desired retrieval process cannot conserve momentum—that is to say it is not phase matched—and the efficiency suffers [24,25]. There are good practical reasons for using systems where states $|1\rangle$ and $|3\rangle$ are nondegenerate, since this renders the bright control and weak signal fields spectrally distinct, and so the above phase-matching issue is relevant to a wide class of possible storage media.

III. PHASE MATCHING

Here we present a scheme that ameliorates the above difficulty, while preserving a large overlap of the spin wave generated by the storage process with the optimal spin wave for retrieval. This allows for high memory efficiency even when the states $|1\rangle$ and $|3\rangle$ have a large energy splitting, so the signal and control fields can be spectrally filtered with high contrast. Furthermore, an angle is introduced between the signal and control beams, so that the two fields may also be spatially filtered.

Phase matching is a well-known problem in nonlinear optics [28], and although complex in general, it becomes simple in atomic vapors, where the absence of natural birefringence removes many of the more involved geometric considerations. Correlations arising from phase-matched light-scattering in gases are routinely used in biomedical and industrial sensing [29,30] and have more recently been used to generate entangled photon pairs [31,32]. We now provide details of a simple phase-matching scheme for the quantum storage problem that addresses the issue of momentum conservation discussed above while keeping the deviations from a collinear geometry small. Let the signal field have wave vectors \mathbf{k}_s and \mathbf{k}'_s at storage and retrieval, respectively. The corresponding control field wave vectors will be denoted by \mathbf{k}_c and \mathbf{k}'_c . The fields need not be collinear, but for simplicity we restrict them to be coplanar. The spin wave generated by the storage process acquires a wave vector $\boldsymbol{\kappa} = \mathbf{k}_s - \mathbf{k}_c$. Upon retrieval, the phase-matching condition $\mathbf{k}'_s = \boldsymbol{\kappa} + \mathbf{k}'_c$ defines the unique direction into which the signal field is emitted with high efficiency [see Fig. 2(a)]. Assuming for the moment that the frequencies of the control and signal fields are fixed, the orientation of \mathbf{k}'_s is completely determined by the angle θ between \mathbf{k}_s and \mathbf{k}_c during storage [33]. It is now necessary to

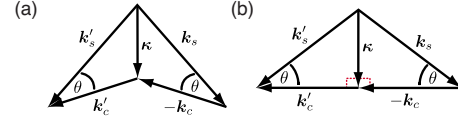


FIG. 2. (Color online) (a) A general phase-matching diagram for the combined storage and retrieval processes. (b) The phase-matching diagram for our proposed scheme.

choose this angle so as to maximize the spatial overlap of the generated and optimal spin waves. That is, we should aim to approximate as nearly as possible collinear storage, followed by backward retrieval. In this arrangement, we operate as close to the dynamic optimum as is compatible with kinematic constraints.

Heuristically, it is clear that choosing θ so that $|\mathbf{k}_s| \cos \theta = |\mathbf{k}_c|$ comes close to satisfying our requirements [see Fig. 2(b)]. Here the signal field is angled so that $\boldsymbol{\kappa}$ is orthogonal to \mathbf{k}_c . When the direction of the control is reversed for retrieval, no phase mismatch is introduced, and the signal field is retrieved at the same angle θ with respect to the retrieval control pulse. We also consider the possibility that the storage state $|3\rangle$ is energetically lower than the initial state $|1\rangle$. In this case, efficient phase-matched retrieval is achieved by choosing θ so that $|\mathbf{k}_c| \cos \theta = |\mathbf{k}_s|$.

The control field couples states $|2\rangle$ and $|3\rangle$, whose populations remain negligible, so it travels at the speed of light c , and we have $|\mathbf{k}_c| = k_c = \omega_c/c$. Interaction with the resonance $|2\rangle$ induces a phase shift on the signal field, however, since it couples to the populated initial state $|1\rangle$, so that $|\mathbf{k}_s| = k_s = \omega_s/c - k_d$, with $k_d = d\gamma\Delta/(\gamma^2 + \Delta^2)L$, where d is the resonant optical depth of the ensemble [25] and L is the ensemble length. Dispersion vanishes exactly on resonance, so for EIT we recover $k_s = \omega_s/c$. For far-detuned Raman storage, the material dispersion is generally small but significant. Our proposed scheme for efficient operation of both EIT and Raman memories is summarized by the choice

$$\theta = \cos^{-1}(r), \quad r = \min\{k_s/k_c, k_c/k_s\}. \quad (1)$$

We have not considered the effects of decoherence on the spin wave during the storage period; in general, it is essential that dissipative processes be effectively eliminated if quantum memories are to become a viable technology. Nonetheless, it should be noted that in memories based on atomic vapor, diffusion of the atoms tends to wash out high spatial frequencies in the amplitude of the spin wave. Therefore, the efficiency of phase-matched retrieval may suffer if $\lambda_{\boldsymbol{\kappa}} = 2\pi/|\boldsymbol{\kappa}| < D$, where D is the distance over which atoms diffuse during the storage time [3,33]. These considerations do not apply to solid-state ensemble memories, however, since the absorbers are stationary.

Although we have used the results of one-dimensional treatments [24,25] to justify the assertion that collinear storage followed by backward retrieval is ideal, we cannot check the performance of our phase-matching scheme using such models. In particular, it is clear that as soon as an angle is introduced between the signal and control fields, walk-off will limit the size of the region over which the fields overlap, and therefore the memory efficiency will depend on the rela-

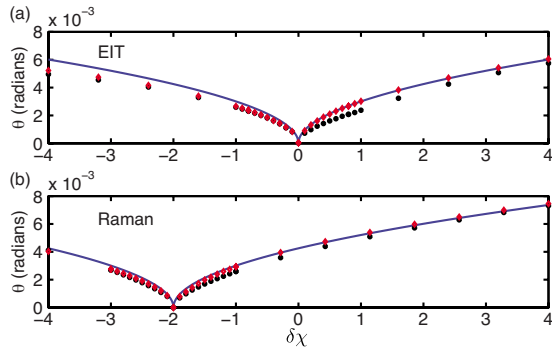


FIG. 3. (Color online) Comparison of numerical results for the optimal angle θ with the prediction in Eq. (1) (solid line). The filled circles correspond to tight control focusing, with $w_c = w_s$; the open diamonds correspond to loose focusing, with $w_c = 2w_s$. We plot the results for a typical EIT protocol in (a): the signal pulse bandwidth is of order γ , the ensemble optical depth is $d=30$. In (b) we present equivalent results for a Raman protocol, with the larger optical depth of $d=300$. The signal bandwidth is of order 10γ and the detuning is $\Delta=150\gamma$.

tive widths of the beams used. To confirm the efficacy of our approach, we performed numerical simulations of the memory interaction in two spatial dimensions. Geometric walk-off, diffraction, and dispersion are correctly modeled, and the efficiency of the combined storage and retrieval process is examined as a function of the splitting $\omega_s - \omega_c$ between the states $|3\rangle$ and $|1\rangle$ for both Raman and EIT memory protocols. We present the results below; details of the numerical model can be found in Appendix B.

IV. RESULTS

We simulated storage, followed by retrieval, according to the geometry specified in Fig. 2(a), over a range of angles θ between the signal and control, and over a range of energy splittings between the states $|1\rangle$ and $|3\rangle$. Below we compare the angles at which the memory efficiency is maximized with our prediction in Eq. (1). We then investigate how these maximal efficiencies compare with the best efficiencies achievable using a collinear geometry.

Figure 3 shows the angle θ at which the combined efficiency of storage followed by phase-matched backward retrieval is optimized, as a function of the phase mismatch $\delta\chi \equiv (\omega_c - \omega_s)L/c$ due to nondegeneracy of the initial and storage states. We borrow parameters from a cesium ensemble memory, with optical frequencies in the near-infrared, and an aspect ratio $\alpha = L/w_s \sim 300$, with w_s the signal beam waist. For an ensemble length of $L \sim 2$ cm, $|\delta\chi| \sim 4$ corresponds roughly to the ground-state hyperfine frequency splitting in cesium, around 10 GHz. The angles in Fig. 3 are extremely small; this level of sensitivity is typical of phase-matched processes. But angle tuning with this degree of precision is possible with conventional optical mounts.

We present the results of two simulation runs: one in which the control beam waist w_c is identical to the signal waist w_s , and one in which the control beam is twice as

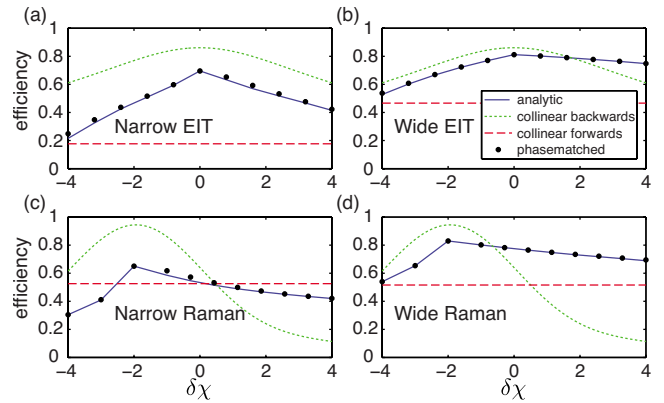


FIG. 4. (Color online) Memory efficiencies versus the phase mismatch $\delta\chi$. (a) and (b) contain the results for the EIT protocol, with tight and loose focusing, respectively. (c) and (d) report the results for the Raman protocol for tight and loose focusing. The solid lines represent the efficiencies achieved if the angles predicted by Eq. (1) are used. The filled circles are the best efficiencies achievable. The dotted lines delimit the optimal efficiency attainable using collinear backwards retrieval, calculated using the one-dimensional theory described in Appendix A. The dashed straight lines denote the efficiencies achieved using collinear forwards retrieval.

wide—with the control pulse energy increased by a factor of 4 so that the control field intensity is the same in both cases. As might be expected, the phase-matching scheme of Eq. (1) correctly predicts the optimal angles for the latter case, where walk-off is mitigated by the loose control focusing. The prediction is less accurate for the former case. The material dispersion in the Raman protocol is responsible for shifting the results so that an optimal angle of $\theta=0$ is obtained for nonzero phase mismatch $\delta\chi$.

Figure 4 shows the variation in the optimal memory efficiency with phase mismatch, for both EIT and Raman protocols with both tight and loose control focusing. We used temporal profiles for the signal fields to be stored that are predicted, by a one-dimensional treatment, to give optimal storage efficiency when $\theta=0$ (see Appendix A for details). Although small improvements over the analytic phase-matching scheme are possible when the control is tightly focused, in general use of the scheme produces near-optimal results. As expected, the memory efficiency is always highest for $\delta\chi$ such that $\theta=0$, since then walk-off is eliminated. The efficiency falls as a phase mismatch is introduced, but there is a marked difference between the behavior for negative and positive $\delta\chi$, corresponding to the storage state $|3\rangle$ lying energetically above and below the initial state $|1\rangle$, respectively. More precisely, the important quantity is the momentum mismatch $\delta\chi + k_d L$; the phase-matching scheme is effective for positive momentum mismatches $\delta\chi > -k_d L$, but it fails when the momentum mismatch is negative, $\delta\chi < -k_d L$. In the EIT protocol, the material dispersion vanishes and effective phase matching requires $\delta\chi > 0$. For the Raman case shown, the ensemble refractive index is significant, and phase matching starts to fail for $\delta\chi \lesssim 2$. This asymmetry is naturally explained by considering the spatial distribution of the spin wave deposited by the signal field as it is stored. In the case

of positive momentum mismatch, the retrieved signal field propagates along the same axis as the stored signal field, and the entire length of the spin wave contributes in the retrieval process. For negative momentum mismatch, as shown in Fig. 2, the retrieved signal field overlaps only partially with the spin wave—which occupies a narrow region parallel to the propagation direction of the stored signal—experiencing commensurately lower gain.

The straight dashed lines in Fig. 4 indicate the efficiency achieved if θ is set to zero, and retrieval is undertaken in the forward direction. This efficiency is generally low, due to poor overlap of the spin wave with the optimal mode for retrieval, but it is independent of the phase mismatch $\delta\chi$, since momentum is automatically conserved in this configuration. Using a one-dimensional analysis, it is possible to predict the signal pulse shape that optimizes the combined efficiency of collinear storage followed by forwards retrieval [25] (see Appendix A for details). For the EIT protocol, these “forward” pulse shapes perform better than the “backward” pulse shapes designed to optimize storage with backward retrieval, and so the “forward” pulse shapes are used in plots (a) and (b) of Fig. 4. However, for the Raman protocol shown, the “forward” pulse shapes perform *worse* than the “backward” pulse shapes, and therefore we used the “backward” pulse shapes in plots (c) and (d). The off-resonant Raman protocol relies on the intense control to mediate the coupling of the signal field to the ensemble, so the memory efficiency is sensitive to diffraction, which reduces the control intensity toward the ends of the ensemble. This explains why the “backward” pulse shapes are more effective for the Raman protocol than the “forward” pulse shapes, since the latter are designed to redistribute the spin wave so that it has a large amplitude toward the back end of the ensemble, and this is precisely where the memory interaction is weakened by diffraction. For wider control beams, with $w_c \geq 2.4w_s$, we verified that the “forward” pulses do indeed perform better than the “backward” pulses, since diffraction becomes negligible. EIT would appear to be less sensitive to diffraction, since small changes in the control intensity modify the signal group velocity, but not the strength of its coupling to the atoms.

The dotted lines in Fig. 4 represent the maximum efficiency achievable for collinear *backward* retrieval, as predicted by a one-dimensional analysis (see Appendix A for details). This efficiency falls rapidly as the momentum mismatch increases. In the case of tight control focusing, diffraction reduces the memory efficiency significantly below the one-dimensional optimum, even for $\theta=0$. When the control is loosely focused, however, the efficiency rises significantly, exceeding the best performance possible with any collinear protocol for large momentum mismatches. Wider control beams allow efficient storage and retrieval at even greater angles; in general, an arbitrarily large positive phase mismatch can be accommodated provided sufficient energy is available to maintain the control intensity required to effect the memory interaction.

In Fig. 5, we combine Figs. 3 and 4, and plot the memory efficiency versus the optimal phase-matching angle. The above simulations demonstrate that the efficiency of ensemble memories can be dramatically improved with the use

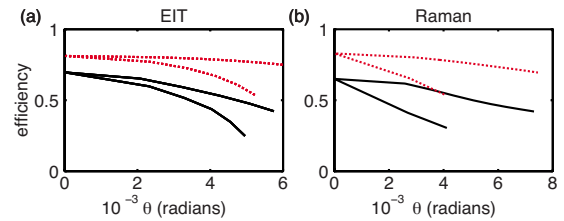


FIG. 5. (Color online) Efficiency versus optimal phase-matching angle. The solid lines correspond to tight control focusing $w_c = w_s$, the dotted lines to looser focusing, with $w_c = 2w_s$. Each line has two “branches”: the upper branch is achieved for positive momentum mismatch, the lower for negative momentum mismatch. The results for the EIT protocol are plotted in (a); those for the Raman protocol in (b).

of noncollinear geometries, and indeed the observed efficiencies, obtained using the formula (1), are close to the best efficiencies achievable with no phase mismatch in a collinear geometry, which represent the dynamical extrema. Nonetheless, an exhaustive search of all possible geometries for storage followed by retrieval is beyond the scope of this work; superior configurations may yet be found.

In summary, our simulations showed that the control should be loosely focused, with a beam waist more than twice that of the signal. In addition, we found that in general positive phase mismatches, where the initial state $|1\rangle$ lies energetically *above* the storage state $|3\rangle$, are preferable.

V. ANGULAR MULTIPLEXING

Having demonstrated the advantages of correct phase matching over collinear operation, namely the combination of high efficiency with spectral and spatial distinguishability of signal and control, we move on to examine the possibilities for multimode storage in ensembles.

Multimode quantum memories can be used to improve the performance of quantum repeaters [34–37], and the ability to store multiple spatial modes in an ensemble allows for novel quantum computing architectures [38]. In the following, we consider using the strong directional selectivity imposed by phase-matching constraints to isolate different spatial modes within the ensemble, such that each mode may be addressed independently of the others. We do not explicitly model multimode storage, since a correct account of coupling between modes requires that we abandon the slowly varying envelope approximation, making the numerics prohibitively time-consuming. But we make an estimate of the multimode capacity of an ensemble memory based on the eikonal approximation that sufficiently different spatial frequencies are dynamically decoupled.

Suppose we want to store a pair of signal pulses in the same ensemble. We can use different angles θ_1, θ_2 between the control and signal fields for storage, so that the resulting spin wave momenta κ_1, κ_2 point in different directions for the two signals. Given some phase mismatch $\delta\chi$, the retrieval process will be phase matched at correspondingly different angles for the two signals. Provided these angles differ sufficiently, a retrieval control pulse for the first signal will

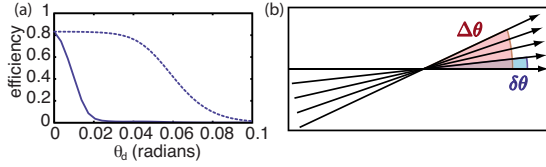


FIG. 6. (Color online) (a) Memory efficiency versus deviation angle θ_d for an EIT protocol with a wide control beam $w_c = 9w_s$. The dotted line corresponds to zero phase mismatch, the solid line to $\delta\chi = 1$. (b) Angular multiplexing. Different signal fields may be stored with different angles θ . Provided the difference $\delta\theta$ in angle between adjacent modes is large enough, the modes are “holographically isolated” and may be addressed, and resolved, independently. The largest angle $\Delta\theta$ for which the memory protocol is acceptably efficient sets a limit to the multimode capacity of such a multiplexed memory.

have a vanishing probability for extracting the second signal, and vice versa. Therefore, the two signals may be addressed *independently* of one another. We can extend this to a larger number of signal modes, each stored with a different angle, and so obtain a multimode memory.

To demonstrate the selectivity afforded by phase matching, we simulated an EIT memory where the storage geometry is determined by our scheme Eq. (1), but where at retrieval the control field angle deviates from the optimal one by θ_d . The variation of the memory efficiency with θ_d is plotted in Fig. 6(a) for the cases $\delta\chi = 0$ and 1. In the former case, the spin wave momentum κ vanishes, and all retrieval angles are phase matched, so the memory efficiency is only limited by walk-off. We used a wide control with $w_c = 9w_s$ so the efficiency remains high over a large range of angles. For the case $\delta\chi = 1$, the spin wave momentum becomes important, and the efficiency falls quickly as the deviation θ_d is increased. Due to the linearity of the memory, this example suffices to show that tuning the angle of the retrieval control field can “switch off” the read-out of one mode, and equally well “switch on” the read-out of another mode. For this example, we should choose $|\theta_2 - \theta_1| = \theta_d \geq 0.02$. Near identical results are reproduced if a Raman protocol is used—in this case, the spin wave momentum vanishes when $\delta\chi = -k_d L$.

In accordance with the results of Sec. IV, the storage efficiency for a given phase-matching angle is maximized for a particular wave vector k_s , which is to say a particular signal frequency ω_s . Signal modes with larger angles may be stored more efficiently by adjusting their center frequencies appropriately. Using the formula (1), we have $\omega_s = \omega_c \cos(\theta) + ck_d$ (for the case $\omega_s < \omega_c$, which is preferable for phase matching). This type of optimization for multimode storage is easily accommodated in the Raman configuration, where the memory efficiency changes slowly with detuning; for EIT storage, such fine-tuning of the mode frequencies is incompatible with the requirement of exact resonance with the state [2].

In order to resolve signal fields propagating at different angles, each signal mode should have an angular divergence smaller than the angular separation $\delta\theta$ of the modes [see Fig. 6(b)]. The angular divergence is limited by diffraction, whence we obtain the condition $\delta\theta \sim \lambda_s / w_s$, where $\lambda_s = 2\pi / k_s$ is the signal field wavelength. The angular separa-

tion should also be sufficient to ensure that there is no “cross-talk” between neighboring modes. This requirement amounts to the condition $w_s k_s \delta\theta \sim 2\pi$ on the transverse optical phase, which again implies $\delta\theta \sim \lambda_s / w_s$. We therefore find that the multimode capacity of a Raman memory is bounded by the number of diffraction-limited signal modes that can be efficiently stored. For the example in Fig. 6(a), we have $\delta\theta \sim 0.01$, which is a reasonable estimate of the angle beyond which efficient retrieval fails when $\delta\chi \neq 0$.

A simple estimate of the multimode capacity for a quantum memory multiplexed in this way is found by taking the ratio $N = \Delta\theta / \delta\theta$, where $\Delta\theta \sim w_c / L$ is the largest angle θ for which efficient storage is possible, as limited by walk-off. We then find that $N \sim w_c w_s / \lambda_s L \sim \mathcal{F}$, with $\mathcal{F} = \sqrt{\mathcal{F}_c \mathcal{F}_s}$ the geometric mean of the Fresnel numbers of the regions illuminated by the control and signal fields. The Fresnel number is known to characterize the number of optical modes supported within a thin pencil-like volume [39]. For the example in Fig. 6(a), we calculate $N \sim 3$. The preceding discussion suggests that both signal and control beams should be loosely focused to achieve a large multimode capacity, with Rayleigh ranges much longer than the ensemble length. Our numerical results show that we should have $w_c \geq 2w_s$ for efficient storage, however, so that the signal modes should always be more tightly focused than the control.

The feasibility of such a multimode memory depends on the ability to produce control pulses of sufficient energy that the coupling remains high even when the control is loosely focused. As a concrete example, consider an ensemble consisting of ~ 2 cm of atomic cesium vapor at 50 °C, with an optical depth $\sim 10^3$ on resonance with the D₂ line at 852 nm. Raman storage is robust to the deleterious effects of Doppler and pressure broadening in this kind of medium, by dint of its large detuning from the optical resonance. The control field is taken from a train of 10 nJ pulses output from a Ti:sapphire oscillator, corresponding to an average power of ~ 1 W with a typical repetition rate of 80 MHz. If the control is focused down to a spot of diameter ~ 7 mm over the ensemble length, with $w_s = w_c / 3$, we calculate a multimode capacity of ~ 100 signal modes, with an average efficiency $\geq 90\%$ (corresponding to $C > 2$, see Appendix A). A more conservative estimate might revise this number downwards by a factor of 10, but this still represents a considerable leap in parallelism over single mode storage.

VI. SUMMARY

In conclusion, we have highlighted a phase-matching problem relevant to all ensemble-based memories that has received little attention in the literature (but see [25]). We have presented a simple solution based on noncollinear storage and retrieval, and examined its applicability numerically. We found good agreement with analytic predictions, and a marked improvement in efficiency over the un-phase-matched case. In addition, we considered the feasibility of multimode storage by angular multiplexing, and found that a large number of modes may be stored with reasonable parameters. As experimental techniques for dealing with ensemble memories mature, we expect these results to be of

use in optimizing the performance and capacity of this technology.

ACKNOWLEDGMENTS

This work was supported by the EPSRC through the QIP IRC (GR/S82716/01) and project EP/C51933/01, and in part by the National Science Foundation under Grant No. NSF PHY05-51164. J.N. thanks Hewlett-Packard for support. I.A.W. was supported in part by the European Commission under the Integrated Project Qubit Applications (QAP) funded by the IST directorate as Contract No. 015848.

APPENDIX A: OPTIMIZATION

It has been shown previously how to optimize the storage efficiency of an ensemble memory in both the Raman and EIT limits [24,25,40]. Here we use an approach that unifies these results. A detailed exposition of the method is reserved for a future work. For now, we simply introduce the principle behind the optimization, and the result. Our aim is to find the optimal temporal profile for an incident signal field, such that it is stored, and then retrieved, with the highest possible probability by given control fields. In practice, it is desirable to solve the reverse problem—to find the optimal temporal profile for the control fields, such that a *given* signal field is optimally stored and retrieved. This is done in the works mentioned above, but it is a slightly harder problem to solve, and solution of the former problem is sufficient for the purposes of our simulations: it is no more difficult to shape the signal than it is the control. To obtain a closed-form expression for the optimal signal profile, we consider propagation in one dimension with $\theta=0$. The memory interaction is linear (as it should be for a quantum memory capable of storing coherent superpositions). Therefore, we may express the temporal profile A_{out} of the retrieved signal field as a function of time τ in terms of the linear mapping,

$$A_{\text{out}}(\tau) = \int_{-\infty}^{\infty} K(\tau, \tau') A_{\text{in}}(\tau') d\tau', \quad (\text{A1})$$

where A_{in} is the temporal profile of the incident signal field, and the integral kernel K is the Green's function for the combined processes of storage and retrieval. In general, K can always be constructed by numerical solution of the equations of motion. In fact, the present discussion applies equally well to a three-dimensional treatment, with transverse coordinates added appropriately, but the numerical construction of a full 3D Green's function remains computationally impractical at present. The efficiency of the memory is given by the modulus square of A_{out} , integrated over all time. The optimization problem, therefore, is reduced to finding the input A_{in} that maximizes the norm of A_{out} . The problem is solved by considering the singular value decomposition [41] of the kernel K ,

$$K(\tau, \tau') = \sum_j \psi_j(\tau) \lambda_j \varphi_j^*(\tau'). \quad (\text{A2})$$

This decomposition exists for any complex bivariate function, provided it is not too pathological, and extremely effi-

cient algorithms exist for finding it. The optimal efficiency is achieved by choosing A_{in} to be the “right singular function” $\varphi_1(\tau)$ that is associated with the largest singular value λ_1 of K . Making use of the adiabatic approximation [24,25], we can obtain an explicit expression for the optimal signal input mode. We introduce the complex detuning $\Gamma = \gamma + i\Delta = i|\Gamma|e^{-i\beta}$. We then define the dimensionless coupling $C = \sqrt{d\gamma W}/|\Gamma|$, and the dimensionless *balance* $R = \sqrt{W/d\gamma}$, where $W = \omega(\tau \rightarrow \infty)$ is the long-time limit of the integrated Rabi frequency $\omega(\tau) = \int_{-\infty}^{\tau} |\Omega(\tau')|^2 \tau'$, with $\Omega(\tau)$ the time-dependent Rabi frequency of the control field. The optimal input mode is then given by

$$\varphi_1(\tau) = e^{i\omega(\tau)\Delta/|\Gamma|^2} \Omega(\tau) \phi_1 \{C[1 - \omega(\tau)/W]\}, \quad (\text{A3})$$

where ϕ_1 is the right singular function associated with the largest singular value of the integral kernel,

$$\tilde{K}(y, y') = \int_0^C k(y, x) k(x, y') e^{2i(\delta\chi + k_d L)x/C} dx, \quad (\text{A4})$$

with

$$k(x, y) = e^{-\sin(\beta)[x/R + Ry]} J_0(2e^{i\beta}\sqrt{xy}), \quad (\text{A5})$$

where x and y are dimensionless coordinates running from 0 up to C , and where J_0 denotes a zeroth-order Bessel function of the first kind. The complex exponential in Eq. (A4) accounts for the momentum mismatch between the stored spin wave and the spin wave mode that correctly phase matches the retrieval process. The kernel \tilde{K} is related to the Green's function K by a unitary transformation, and therefore the singular values λ_j of K are the same as the singular values of \tilde{K} .

The formula (A3) is valid under adiabatic conditions for arbitrary detunings, so that it can be used in both EIT and Raman protocols. Adiabaticity requires that the bandwidth δ and the peak Rabi frequency Ω of the control field are not too large, so that “ringing” effects, such as oscillations between the states $|2\rangle$ and $|3\rangle$, are eliminated. For a Raman memory, the detuning guarantees adiabaticity, provided that we have $\{\Omega, \delta\} \ll \Delta$. For EIT, the condition becomes $\{\Omega, \delta\} \ll d\gamma$. It can be shown that both of these conditions are fulfilled, in general, if we ensure that $d\gamma \gg \delta$ [25], which condition is satisfied throughout this paper. Equation (A3) reduces to the results in [24] in the off-resonant limit $\beta \ll 1$, with $\beta C \ll R \ll 1/\beta C$. The results in [25] are reproduced in the limit of large control pulse energy, $R \gg 1$, with $R \gg 1/\beta C$. The phase factor in Eq. (A3) accounts for the dynamic Stark shift induced by the control field; it vanishes on resonance, but it can be important for Raman storage. The dotted lines in Fig. 4 are generated by calculating the efficiency $\eta_{\text{coll}} = \lambda_1^2$ for each value of the phase mismatch $\delta\chi$. They represent the best efficiency achievable by a collinear protocol with backward retrieval.

The temporal profile of the signal pulses used for phase-matched backward retrieval in the simulations is set by using Eq. (A3) with the phase factor in Eq. (A4) omitted; the phase-matching scheme of Eq. (1) eliminates the momentum

mismatch so this choice of input profile is close to optimal, notwithstanding diffraction and walk-off effects, which are neglected in the above treatment.

In the case of collinear storage followed by forward retrieval, the predicted optimal pulse shape is given by Eq. (A3), except that the second kernel in the integrand of Eq. (A4), $k(x, y')$, is replaced by $k(C-x, y')$, and the exponential phase factor is omitted. As mentioned in the main text, these “forward” pulse shapes are of limited value for the Raman protocol operated with a tightly focused control, due to diffraction effects unaccounted for in this one-dimensional model.

APPENDIX B: NUMERICAL MODEL

To proceed with a numerical analysis of the quantum memory interaction, we consider the propagation of signal and control fields in the (x, z) plane in the presence of a Λ -type atomic medium [33,42]. Quantum fluctuations [43,44] do not influence the efficiency of the memory, so the dynamics are adequately described by classical equations of motion. The z axis is defined by the direction of propagation of the signal field. We transform to a frame moving with the signal pulse and define the local time $\tau = t - z/v$, where t is the time in the laboratory frame and v is the signal pulse velocity. The linearized Maxwell-Bloch equations describing the quantum memory interaction are then given, in the slowly varying envelope approximation, by [24,25,43]

$$\begin{aligned} \left[\frac{\alpha^2}{2i\bar{k}_s} \partial_x^2 + \partial_z \right] A &= i\sqrt{d}\gamma P, \\ \partial_\tau P &= -\Gamma P + i\sqrt{d}\gamma A + i\Omega B, \\ \partial_\tau B &= i\Omega^* P. \end{aligned} \quad (\text{B1})$$

Here A and B are the slowly varying amplitudes of the signal field and spin wave, respectively. The slowly varying Rabi frequency Ω represents the control field envelope and P denotes the slowly varying amplitude of the atomic polarization on the $|1\rangle \leftrightarrow |2\rangle$ transition. The various constants are defined as follows. d is the resonant optical depth of the ensemble along the z axis, 2γ is the homogeneous linewidth of the $|1\rangle \leftrightarrow |2\rangle$ transition, $\Gamma = \gamma + i\Delta$ is the complex detuning, $\alpha = L/w_s$ is the aspect ratio of the ensemble, with L its length along the z axis, and w_s is the beam waist of the signal field. $\bar{k}_s = |\mathbf{k}_s|L$ is the dimensionless magnitude of the signal field wave vector, and the signal pulse velocity $v = cT_c/L$ is the dimensionless speed of light, with T_c a time scale set by the duration of the control field. The frequencies γ , Ω , and Γ are all rendered dimensionless by expressing them in units of $1/T_c$. In accordance with the above normalizations, the coordinates are scaled so that the longitudinal position z , the transverse position x , and the local time τ are expressed in units of L , w_s , and T_c , respectively. In these units, z runs from $-\frac{1}{2}$ to $\frac{1}{2}$; x and τ both from around -3 to 3 —a limit chosen to be sufficiently large to capture all significant dynamics, while small enough to obtain results in practicable time.

The coupled system (B1) is solved by finite differences using the method of lines [45]. We employ spectral collocation to approximate the spatial derivatives ∂_x and ∂_z —replacing them with Chebyshev differentiation matrices [46]. The time evolution is then generated using a second-order partially implicit Runge-Kutta formula. We discretize the (x, z) plane on a 21×21 grid, which affords accuracy to machine precision. We use around 500 time steps, which guarantees convergence and provides accuracy to around 10^{-3} . We verified that near identical results are achieved with a 9×9 spatial grid, and 100 time steps. We use a Gaussian transverse spatial profile for the signal field to be stored; the temporal profile is determined using the one-dimensional optimization described previously in Appendix A. The signal field at the input face of the ensemble is given by

$$A\left(z = -\frac{1}{2}, x, \tau\right) = \exp\left\{-\left[\frac{x}{W_s\left(-\frac{1}{2}\right)}\right]^2 + \frac{i\bar{k}_s x^2}{2R_s\left(-\frac{1}{2}\right)}\right\} \times \varphi_1(\tau), \quad (\text{B2})$$

where $W_s(z) = \sqrt{1 + (z/z_s)^2}$ is the signal beam size, $R_s(z) = \alpha^2 z [1 + (z/z_s)^2]$ is the signal phase curvature, and $z_s = \bar{k}_s / (2\alpha^2)$ is the signal Rayleigh range. Note that the amplitude of A is arbitrary, since the system (B1) is manifestly linear. We use Gaussian temporal and spatial profiles for the storage and retrieval control pulses. The control pulse is launched with amplitude Ω_0 at an angle θ to the z axis,

$$\begin{aligned} \Omega(z, x, \tau) &= \Omega_0 \times \frac{w_c}{W_c(z')} \exp\left\{-\left[\frac{x'}{W_c(z')}\right]^2 + \frac{i\bar{k}_c x'^2}{2R_c(z')}\right\} \\ &\times \exp\{-[\tau - \tau_0 + (z - z')/v]^2\}, \end{aligned} \quad (\text{B3})$$

where x' and z' are transformed coordinates given by

$$\begin{aligned} x' &= \cos(\theta)x + \alpha \sin(\theta)z, \\ z' &= \cos(\theta)z - \frac{\sin(\theta)}{\alpha}x, \end{aligned} \quad (\text{B4})$$

where the factors of α appear to account for the different normalizations of the longitudinal and transverse coordinates. Here $\bar{k}_c = |\mathbf{k}_c|L$ is the dimensionless magnitude of the control field wave vector, $W_c(z) = w_c \sqrt{1 + (z/z_c)^2}$ is the control beam size, $R_c(z) = \alpha^2 z [1 + (z/z_c)^2]$ is the control phase curvature, and $z_c = \bar{k}_c w_c^2 / (2\alpha^2)$ is the control Rayleigh range, with w_c the control beam waist, expressed in units of w_s . τ_0 sets the control pulse timing, in units of T_c ; we adjust τ_0 so that the signal field, whose temporal profile is determined from the control via Eq. (A3), is centered in the temporal domain of our simulations. In the simulations presented in the main text, the control amplitude was set to $\Omega_0 = 5$. We used $L = 2$ cm and $T_c = 300$ ps for Raman storage, and $T_c = 3$ ns for EIT, with $1/\gamma = 3$ ns in both cases.

The storage efficiency is calculated as the ratio of stored to incident energy,

$$\eta_{\text{store}} = \frac{\int_{-\infty}^{\infty} \int_{-1/2}^{1/2} |B(x, z, \tau \rightarrow \infty)|^2 dz dx}{\int_{-\infty}^{\infty} \int_{-\infty}^{\infty} \left| A\left(x, z = -\frac{1}{2}, \tau\right) \right|^2 d\tau dx}. \quad (\text{B5})$$

Having simulated the storage process, we transform our coordinate system so that the z axis for the retrieval process coincides with the direction in which the signal field generation is phase matched. The spin wave at the start of the retrieval process is related to the spin wave at the end of the storage process by the transformation

$$[B(z, x, \tau \rightarrow -\infty)]_{\text{retrieval}} = [B(z', x', \tau \rightarrow \infty)]_{\text{storage}}, \quad (\text{B6})$$

where z' , x' are as defined in Eq. (B4), except that the angle θ is replaced by

$$\theta' = -2 \sin^{-1} \left[\frac{\bar{k}_c \sin(\theta)}{\sqrt{\bar{k}_s^2 + \bar{k}_c^2 - 2\bar{k}_c \bar{k}_s \cos(\theta)}} \right]. \quad (\text{B7})$$

As can be seen from Fig. 2(a), the retrieval control field is launched at an angle $-\theta$ to the z axis for the retrieval process. The retrieval efficiency is calculated as the ratio of retrieved to stored energy,

$$\eta_{\text{retrieve}} = \frac{\int_{-\infty}^{\infty} \int_{-\infty}^{\infty} \left| A\left(x, z = \frac{1}{2}, \tau\right) \right|^2 d\tau dx}{\int_{-\infty}^{\infty} \int_{-1/2}^{1/2} |B(x, z, \tau \rightarrow -\infty)|^2 dz dx}. \quad (\text{B8})$$

Finally the total efficiency η_{total} for storage followed by retrieval (neglecting, as we have, any decoherence of the spin wave) is just given by the product of the separate efficiencies, $\eta_{\text{total}} = \eta_{\text{store}} \eta_{\text{retrieve}}$.

-
- [1] M. Fleischhauer, A. Imamoglu, and J. Marangos, *Rev. Mod. Phys.* **77**, 633 (2005).
- [2] T. Fernholz *et al.*, e-print arXiv:0802.2876.
- [3] K. Surmacz *et al.*, *Phys. Rev. A* **74**, 050302 (2006).
- [4] D. N. Matsukevich, T. Chaneliere, M. Bhattacharya, S. Y. Lan, S. D. Jenkins, T. A. B. Kennedy, and A. Kuzmich, *Phys. Rev. Lett.* **95**, 040405 (2005).
- [5] K. S. Choi, H. Deng, J. Laurat, and H. J. Kimble, *Nature (London)* **452**, 67 (2008).
- [6] R. Ursin *et al.*, *Nature* **430**, 849 (2004).
- [7] L. Zhang, C. Silberhorn, and I. A. Walmsley, *Phys. Rev. Lett.* **100**, 110504 (2008).
- [8] S. D. Barrett, P. P. Rohde, and T. M. Stace, e-print arXiv:0804.0962.
- [9] N. Sangouard, C. Simon, M. Afzelius, and N. Gisin, *Phys. Rev. A* **75**, 032327 (2007).
- [10] N. B. Phillips, A. V. Gorshkov, and I. Novikova, e-print arXiv:0805.3348v1.
- [11] O. Mishina, N. Larionov, A. Sheremet, I. Sokolov, and D. Kupriyanov, e-print arXiv:0805.3353v1.
- [12] G. Hetet, J. Longdell, A. Alexander, P. Lam, and M. Sellars, e-print arXiv:quant-ph/0612169.
- [13] A. Kalachev and S. Kroll, e-print arXiv:0804.0421.
- [14] S. Moiseev, V. Tarasov, and B. Ham, *J. Opt. B: Quantum Semiclassical Opt.* **5**, S497 (2003).
- [15] D. V. Vasilyev, I. V. Sokolov, and E. S. Polzik, *Phys. Rev. A* **77**, 020302(R) (2008).
- [16] C. A. Muschik, K. Hammerer, E. S. Polzik, and J. I. Cirac, *Phys. Rev. A* **73**, 062329 (2006).
- [17] Z. Kurucz and M. Fleischhauer, e-print arXiv:0712.2400.
- [18] K. Hammerer, A. Sorensen, and E. Polzik, e-print arXiv:0807.3358.
- [19] M. Fleischhauer and M. D. Lukin, *Bull. Am. Phys. Soc.* **65**, 022814 (2002).
- [20] A. V. Gorshkov, A. Andre, M. Fleischhauer, A. S. Sorensen, and M. D. Lukin, *Phys. Rev. Lett.* **98**, 123601 (2007).
- [21] T. Chaneliere, D. N. Matsukevich, S. D. Jenkins, S. Y. Lan, R. Zhao, T. A. B. Kennedy, and A. Kuzmich, *Phys. Rev. Lett.* **98**, 113602 (2007).
- [22] J. Laurat *et al.*, *New J. Phys.* **9**, 207 (2007).
- [23] A. E. Kozhekin, K. Mølmer, and E. Polzik, *Phys. Rev. A* **62**, 033809 (2000).
- [24] J. Nunn *et al.*, *Phys. Rev. A* **75**, 011401 (2007).
- [25] A. V. Gorshkov, A. Andre, M. D. Lukin, and A. S. Sorensen, *Phys. Rev. A* **76**, 033805 (2007).
- [26] I. Novikova, A. V. Gorshkov, D. F. Phillips, A. S. Sorensen, M. D. Lukin, and R. L. Walsworth, *Phys. Rev. Lett.* **98**, 243602 (2007).
- [27] I. Novikova, N. B. Phillips, and A. V. Gorshkov, e-print arXiv:0805.1927v1.
- [28] P. J. Mosley, J. S. Lundeen, B. J. Smith, P. Wasylczyk, A. B. Uren, C. Silberhorn, and A. I. Walmsley, *Phys. Rev. Lett.* **100**, 133601 (2008).
- [29] Y. Shen, *The Principles of Nonlinear Optics* (Wiley-Interscience, Hoboken, NJ, 2003).
- [30] I. W. Schie *et al.*, *Opt. Express* **16**, 2168 (2008).
- [31] S. Du, P. Kolchin, C. Belthangady, G. Y. Yin, and S. E. Harris, *Phys. Rev. Lett.* **100**, 183603 (2008).
- [32] D. A. Braje, V. Balić, S. Goda, G. Y. Yin, and S. E. Harris, *Phys. Rev. Lett.* **93**, 183601 (2004).
- [33] P. Arve, P. Jänes, and L. Thylén, *Phys. Rev. A* **69**, 063809 (2004).
- [34] C. Simon, H. de Riedmatten, M. Afzelius, N. Sangouard, H. Zbinden, and N. Gisin, *Phys. Rev. Lett.* **98**, 190503 (2007).
- [35] N. Sangouard *et al.*, *Phys. Rev. A* **77**, 062301 (2008).
- [36] O. A. Collins, S. D. Jenkins, A. Kuzmich, and T. A. B. Kennedy, *Phys. Rev. Lett.* **98**, 060502 (2007).
- [37] M. Afzelius, C. Simon, H. de Riedmatten, and N. Gisin, e-print arXiv:0805.4164.
- [38] K. Tordrup, A. Negretti, and K. Molmer, *Phys. Rev. Lett.* **101**, 040501 (2008).
- [39] M. G. Raymer, I. A. Walmsley, J. Mostowski, and B. Sobolewska, *Phys. Rev. A* **32**, 332 (1985).
- [40] A. V. Gorshkov, T. Calarco, M. D. Lukin, and A. S. Sorensen,

- Phys. Rev. A **77**, 043806 (2008).
- [41] L. Trefethen and D. Bau, *Numerical Linear Algebra* (SIAM, Philadelphia, 1997).
- [42] G. Nikoghosyan, Eur. Phys. J. D **36**, 119 (2005).
- [43] M. G. Raymer and J. Mostowski, Phys. Rev. A **24**, 1980 (1981).
- [44] P. Kolchin, Phys. Rev. A **75**, 033814 (2007).
- [45] L. Trefethen, unpublished text, available at <http://web.comlab.ox.ac.uk/oucl/work/nick.trefethen/pdetext.html> (1996).
- [46] L. Trefethen, *Spectral Methods in MATLAB* (SIAM, Philadelphia, 2000).